Received August 31, 2020, accepted September 30, 2020, date of publication October 6, 2020, date of current version October 20, 2020.
*Digital Object Identifier 10.1109/ACCESS.2020.3028929*

# An Optimum Volumetric Array Design Approach for Both Azimuth and Elevation Isotropic DOA Estimation

**FESIH KESKIN AND TANSU FILIK**
Department of Electrical and Electronics Engineering, Eskisehir Technical University, 26555 Eskisehir, Turkey
Corresponding author: Fesih Keskin (fesihkeskin@eskisehir.edu.tr)

This work was supported by the Eskisehir Technical University Scientific Research Projects Council under Grant 19ADP102.

**ABSTRACT** In this study, a new volumetric array design approach is presented for both azimuth and elevation isotropic direction of arrival (DOA) estimation. The presented method uses a minimum number of additional sensors to extend the given arrays to a volumetric array which has equal values for the Cramér-Rao lower bound (CRLB) for the entire azimuth and elevation angles. This approach can be applied to all arbitrary linear and planar arrays. Moreover, the design approach also takes into account the electromagnetic mutual coupling (MC) effect between the array elements and both the azimuth and elevation angular ambiguity uncertainties in an optimum manner while extending the array. It has been verified both analytically and with simulations that the designed volumetric arrays satisfy the two dimensional (2-D) isotropic DOA estimation conditions. The proposed approach is applied to Uniform Linear Arrays (ULA), Uniform Circular Arrays (UCA), V-shaped Arrays, and an arbitrary planar array to extend to optimum volumetric arrays with considerable results.

**INDEX TERMS** 2-D isotropic array, 3-D arrays, angular ambiguity, array signal processing, direction of arrival, DOA, mutual coupling, sensor array design, volumetric arrays.

## I. INTRODUCTION

Design of optimum array geometry for the best DOA estimation is widely studied in the literature for decades, and generally, CRLB [1], [2] and the angular ambiguity functions [3], [4] are used together or separately as the performance criteria of the design. CRLB gives the ultimate performance of an unbiased DOA estimation, and the angular ambiguity functions are used to measure the similarities of manifold vectors of a given array for different angles. The primary purpose of practical applications on the sensor array geometry design is to get a minimum and same values of the CRLB for all azimuth angles while maintaining the angular ambiguity within a tolerable level. These arrays are known as isotropic planar arrays, which give an isotropic performance for only azimuth angles [5]–[12]. Since these arrays are planar, their elevation angle estimations are not isotropic.

In recent years, the positioning and tracking of multiple mobile users for the next generation's dense radio access networks are becoming important requirements [13]. Similarly, the amateur small unmanned aerial vehicles, also known as drones, have been a high concern for public safety. Hence the geo-localization and tracking of these drones are critical [14], [15]. In all these problems, the sources are mobile, and both the azimuth and elevation angles should be accurately and quickly estimated. Planar array geometries are insufficient to meet these new and compelling requirements. For both azimuth and elevation isotropic DOA estimation, two dimensional (2-D) isotropic volumetric arrays are defined in [6]. Therefore, it is critically important to find an optimum approach to extend an arbitrary planar array into 2-D isotropic volumetric arrays for the best 2-D DOA estimation. In [17], the effects of the adding sensors to the vertical plane are considered and different volumetric array geometries are analyzed. In [8], the same problem is investigated for the multiple-input multiple-output (MIMO) radar systems. In [9], CRLB based isotropic and directional array design approach with a sensor selection strategy with adaptive array thinning is proposed. In [18], Joint 2-D DOA estimation performance of 3-D L-shaped antenna array design was compared with some well-known planar arrays in terms of detection rate.

The associate editor coordinating the review of this manuscript and approving it for publication was Mohammad Tariqul Islam.

In all these aforementioned studies, the proposed arrays and design approaches have approximately 2-D isotropic performances. Their azimuth and elevation CRLB levels are not exactly equal for all angles. In this paper, a new optimum volumetric array design approach, which extends arbitrary planar arrays to both azimuth and elevation isotropic volumetric arrays with a minimum number of additional sensors, is presented. The presented two-step design approach guaranties to satisfy 2-D isotropic conditions while minimizing both the azimuth and elevation angular ambiguity function subject to the constraint of the mutual coupling effect in an optimum manner. This volumetric array extension approach is applied for well known ULA, UCA, V-shaped array, and an arbitrary planar array with considerable performance improvements. The extended 3-D V-shaped array's 2-D MUSIC spectrum is also compared with the planar V-shaped array in simulations to show the improvements in elevation estimation.

This paper is structured into five sections. Section II briefly describes the data model and general CRLB expressions for arbitrary arrays. In Section III, the 2-D isotropic volumetric sensor array design approach for any given arbitrary linear and planar arrays is presented. Section IV provides the simulation results to verify the effectiveness of the proposed method. Finally, section V concludes the paper.

*Notations:* We use bold small letters to denote vectors and uppercase boldface letters to denote matrices. $\mathbf{1}_M$ and $\mathbf{0}_M$ denote a row vector of $M$ ones and zeros, respectively. $\|\bullet\|$ represents two norm. $\mathbf{I}_M$ denotes $M\times M$ identity matrix. The operators $(\bullet)^T$ and $(\bullet)^H$ denote the transpose and conjugate-transpose of a vector or a matrix, respectively.

## II. PROBLEM FORMULATION

### A. DATA MODEL

We assume an array geometry composed of $M$ identical and omnidirectional sensors located at the positions $\mathbf{p}_m = [x_m\ y_m\ z_m]^T$, $m = 1, \ldots, M$. We consider that $L$ narrowband and far-field source signals are impinging on the array from the directions $(\phi_l,\ \theta_l)$, $l = 1, \ldots, L$, where $\phi \in [0°,\ 180°]$ and $\theta \in [0°,\ 90°]$ denote source azimuth and elevation angles, respectively as shown in Fig. 1. $\phi$ is measured as a counter-clockwise from the positive $x$-axis on the $x$-$y$ plane, while $\theta$ is the clockwise angle made with the positive $z$-axis. The array output, $\mathbf{y}(t)$, at time $t$ can be modeled by,

$$\mathbf{y}(t) = \mathbf{A}\mathbf{s}(t) + \mathbf{n}(t), \quad t = 1, \ldots, T \tag{1}$$

where $T$ is the number of snapshots. The source signal; $\boldsymbol{s(t)}$ is $L\times 1$ vector, $\boldsymbol{y(t)}$ and the noise, $\boldsymbol{n(t)}$ are $M\times 1$ vectors. It is assumed that the signal and noise are uncorrelated, zero-mean, spatially and temporally white Gaussian complex random processes. $\mathbf{A}$ is $M\times L$ steering matrix,

$$\mathbf{A} = [\mathbf{a}(\phi_1, \theta_1),\ \mathbf{a}(\phi_2, \theta_2),\ \cdots,\ \mathbf{a}(\phi_L, \theta_L)] \tag{2}$$

where $\mathbf{a}(\phi_l,\ \theta_l)$ is the $M\times 1$ steering vector of the sensor array in direction $(\phi_l,\ \theta_l)$ as,

$$\mathbf{a}(\phi_l,\ \theta_l) = \left[e^{\{j\mathbf{k}_l{}^T\cdot\mathbf{p}_1\}}\ \ldots\ e^{\{j\mathbf{k}_l{}^T\cdot\mathbf{p}_M\}}\right]^T \tag{3}$$

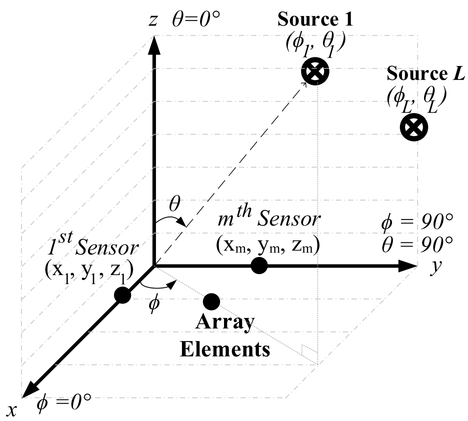


**FIGURE 1. Coordinate system for 2-D DOA estimation.**

where $\mathbf{k}_l = (2\pi f_c \mathbf{u}_l)/c = (2\pi\mathbf{u}_l)/\lambda$ is the wave-number vector in the direction $(\phi_l,\ \theta_l)$, and $\lambda$, $c$, and $f_c$ denote the wavelength, propagation speed of wave, and carrier frequency, respectively. The unit vector pointing towards the source signal directions $(\phi_l, \theta_l)$ is,

$$\mathbf{u}_l = [\sin\theta_l \cos\phi_l\ \ \sin\theta_l \sin\phi_l\ \ \cos\theta_l]^T \tag{4}$$

The output covariance matrix, $\mathbf{R}$, is

$$E\{\mathbf{y}(t)\,\mathbf{y}(t)^H\} = \mathbf{R} = \mathbf{A}\mathbf{R}_s\mathbf{A}^H + \sigma_n^2\mathbf{I}_M \tag{5}$$

where $E\{\bullet\}$ denotes the expectation operator and $\mathbf{R}_s$ is the source correlation matrix.

### B. CRLB EXPRESSION OF ARBITRARY ARRAYS FOR DOA ESTIMATION

The CRLB gives a lower bound on the variance of any unbiased estimator. The azimuth and elevation angle estimators variances should satisfy the following inequalities respectively,

$$var\left(\widehat{\phi}\right) \geq \left[\mathbf{F}^{-1}\right]_{11}, \quad var\left(\widehat{\theta}\right) \geq \left[\mathbf{F}^{-1}\right]_{22} \tag{6}$$

where Fisher information matrix (FIM), $\mathbf{F}$, is given in [1] as,

$$\mathbf{F} = \begin{bmatrix} \mathbf{F}_{\phi\phi} & \mathbf{F}_{\phi\theta} \\ \mathbf{F}_{\theta\phi} & \mathbf{F}_{\theta\theta} \end{bmatrix} \tag{7}$$

The elements of $\mathbf{F}$ can be calculated by,

$$\mathbf{F}_{\phi\phi} = T \times tr\left\{\mathbf{R}^{-1}\frac{\partial\mathbf{R}}{\partial\phi}\mathbf{R}^{-1}\frac{\partial\mathbf{R}}{\partial\phi}\right\} \tag{8}$$

$$\mathbf{F}_{\phi\theta} = T \times tr\left\{\mathbf{R}^{-1}\frac{\partial\mathbf{R}}{\partial\phi}\mathbf{R}^{-1}\frac{\partial\mathbf{R}}{\partial\theta}\right\} \tag{9}$$

where $tr\{\cdot\}$ denotes trace of the matrix and $T$ is the number of snapshots. Thus,

$$\mathbf{F}_{\phi\phi} = \frac{2T}{\sigma_n^2}\Re\left\{\left(\mathbf{R}_s\mathbf{A}^H\mathbf{R}^{-1}\mathbf{A}\mathbf{R}_s\right) \odot \left(\dot{\mathbf{A}}_\phi^H\mathbf{P}_\mathbf{A}^\perp\mathbf{R}^{-1}\dot{\mathbf{A}}_\phi\right)\right\} \tag{10}$$

$$\mathbf{F}_{\phi\theta} = \frac{2T}{\sigma_n^2}\Re\left\{\left(\mathbf{R}_s\mathbf{A}^H\mathbf{R}^{-1}\mathbf{A}\mathbf{R}_s\right) \odot \left(\dot{\mathbf{A}}_\phi^H\mathbf{P}_\mathbf{A}^\perp\mathbf{R}^{-1}\dot{\mathbf{A}}_\theta\right)\right\} \tag{11}$$

where $\Re\{x\}$ denotes real part of $x$ and $\odot$ is the Hadamard (or elementwise) product. Note that $\mathbf{F}_{\theta\theta}$ can be written similar to (10). $\mathbf{F}_{\theta\phi} = \mathbf{F}_{\phi\theta}$ and,

$$\mathbf{P}_{\mathbf{A}}^{\perp} = \mathbf{I}_M - \mathbf{A}\left(\mathbf{A}^H\mathbf{A}\right)^{-1}\mathbf{A}^H, \quad \dot{\mathbf{A}}_{\phi}^{H} = \sum_{l=1}^{L}\frac{\partial \mathbf{A}}{\partial \phi_l} \tag{12}$$

where $\mathbf{P}_{\mathbf{A}}^{\perp}$ is the orthogonal projection of column space of steering matrix $\mathbf{A}$. CRLB expressions for azimuth and elevation estimators are given in [6] as,

$$CRLB(\phi) = \frac{1}{J_{\phi\phi}}\left(1 - \frac{J_{\phi\theta}^2}{J_{\phi\phi}J_{\theta\theta}}\right)^{-1} \tag{13}$$

$$CRLB(\theta) = \frac{1}{J_{\theta\theta}}\left(1 - \frac{J_{\phi\theta}^2}{J_{\phi\phi}J_{\theta\theta}}\right)^{-1} \tag{14}$$

where $J_{\phi\phi} = \sqrt{tr\left(\mathbf{F}_{\phi\phi}\right)/L}$. $J_{\phi\theta}$, $J_{\theta\phi}$, and $J_{\theta\theta}$ can be written in a similar manner.

## III. 2-D ISOTROPIC VOLUMETRIC ARRAY DESIGN

In this section, a new array design approach, which extends the given arbitrary planar array to volumetric arrays to satisfy the 2-D isotropic DOA estimation conditions, is presented. It is assumed that any arbitrary planar array with $M$ sensors is located on the $x$-$y$ plane as

$$\mathbf{x} = [x_1\, x_2 \ldots x_M],\ \mathbf{y} = [y_1\, y_2 \ldots y_M],\ \mathbf{z} = [\mathbf{0}_M] \tag{15}$$

An arbitrary array's moment-of-inertia matrix, $\mathbf{I}_p$, is defined in [19]–[21] as,

$$\mathbf{I}_p = \begin{bmatrix} I_{xx} & I_{xy} & I_{xz} \\ I_{xy} & I_{yy} & I_{yz} \\ I_{xz} & I_{yz} & I_{zz} \end{bmatrix} \tag{16}$$

where $I_{xy}$, $I_{xz}$, and $I_{yz}$ represent the cross moment-of-inertia (off-diagonal elements) and $I_{xx}$, $I_{yy}$, and $I_{zz}$ represent the auto moment-of-inertia (diagonal elements) of $x$, $y$ and $z$ coordinates, respectively. The matrix elements of (16) are calculated as,

$$I_{xy} = \left(\mathbf{x} - \mu_{\mathbf{x}}\mathbf{1}_M\right)\left(\mathbf{y} - \mu_{\mathbf{y}}\mathbf{1}_M\right)^T \tag{17}$$

$$I_{xz} = \left(\mathbf{x} - \mu_{\mathbf{x}}\mathbf{1}_M\right)\left(\mathbf{z} - \mu_{\mathbf{z}}\mathbf{1}_M\right)^T \tag{18}$$

$$I_{yz} = \left(\mathbf{y} - \mu_{\mathbf{y}}\mathbf{1}_M\right)\left(\mathbf{z} - \mu_{\mathbf{z}}\mathbf{1}_M\right)^T \tag{19}$$

$$\begin{aligned} I_{xx} &= \|\mathbf{x} - \mu_{\mathbf{x}}\mathbf{1}_M\|^2,\ I_{yy} = \|\mathbf{y} - \mu_{\mathbf{y}}\mathbf{1}_M\|^2 \\ I_{zz} &= \|\mathbf{z} - \mu_{\mathbf{z}}\mathbf{1}_M\|^2 \end{aligned} \tag{20}$$

where the mean of coordinates is defined as,

$$\mu_{\mathbf{x}} = \left(\mathbf{x}\mathbf{1}_M^T\right)/M,\ \mu_{\mathbf{y}} = \left(\mathbf{y}\mathbf{1}_M^T\right)/M,\ \mu_{\mathbf{z}} = \left(\mathbf{z}\mathbf{1}_M^T\right)/M \tag{21}$$

For the given arbitrary arrays, if $\mathbf{I}_p$ in (16) is a scaled identity matrix then it is a 2-D isotropic array [10]. Thereby, 2-D isotropic conditions in [6], [8] are given as,

$$I_{xy} = I_{xz} = I_{yz} = 0 \tag{22}$$

$$I_{xx} = I_{yy} = I_{zz}. \tag{23}$$

Fig. 2 shows the uniform linear array (ULA), uniform circular array (UCA), and V-shaped array all with a number of five sensors, respectively. These arrays are known as linear and centrosymmetric (planar) arrays and they are located on the $x$-$y$ plane (there is no sensor on $z$ plane). Hence $\mu_{\mathbf{z}}$, $I_{zz}$, $I_{xz}$, $I_{yz}$, and $I_{xy}$ are all zero for these arrays. On the other hand, Fig. 3 shows an arbitrary planar array with four sensors where $\mu_{\mathbf{z}}$, $I_{zz}$, $I_{xz}$, and $I_{yz}$ are zero but $I_{xy}$ is not zero.

Here, we propose the two-step method that can extend all given linear, centrosymmetric (Fig. 2) and non-symmetric arbitrary planar arrays (Fig. 3) to volumetric arrays which satisfy the 2-D isotropic DOA estimation conditions in (22) and (23) by adding a minimum number of sensors.

### A. STEP-1

This step simply checks if the given planar array's cross moment-of-inertia, $I_{xy}$, is zero or not. If it is already zero, there is no need to add a new sensor to the $x$-$y$ plane and we can proceed to the second step directly. Otherwise, we should add a new sensor to the $x$-$y$ plane to make $I_{xy}$ zero. Since the $I_{xy}$'s of the linear and planar arrays in Fig. 2 are zero, we will move on to the second step for these arrays. But for the planar array in Fig. 3, the $I_{xy}$ is not zero. In this case, we have to add a new sensor with coordinate $(\zeta_x, \zeta_y)$ which makes $I_{xy} = 0$. After adding the new sensor, the updated planar array coordinates are,

$$\mathbf{x}^{(1)} = [\mathbf{x}\ \zeta_x],\ \mathbf{y}^{(1)} = \left[\mathbf{y}\ \zeta_y\right],\ \mathbf{z}^{(1)} = [\mathbf{z}\ 0] \tag{24}$$

where $(\cdot)^{(1)}$ denotes the updated parameter at the first step. The updated $I_{xy}^{(1)}$ is obtained as (the derivation details are in Appendix VI-A),

$$\begin{aligned} I_{xy}^{(1)} = \mathbf{x}\mathbf{y}^T + \frac{M}{M^{(1)}}\zeta_x\zeta_y - \frac{M^2}{M^{(1)}}\mu_{\mathbf{x}}\mu_{\mathbf{y}} - \frac{M}{M^{(1)}}\mu_{\mathbf{y}}\zeta_x \\ - \frac{M}{M^{(1)}}\mu_{\mathbf{x}}\zeta_y \end{aligned} \tag{25}$$

where $M^{(1)} = M + 1$. $\mu_{\mathbf{x}^{(1)}}$ and $\mu_{\mathbf{y}^{(1)}}$ are the updated mean of coordinates,

$$\mu_{\mathbf{x}^{(1)}} = \frac{M\mu_{\mathbf{x}} + \zeta_x}{M^{(1)}},\quad \mu_{\mathbf{y}^{(1)}} = \frac{M\mu_{\mathbf{y}} + \zeta_y}{M^{(1)}} \tag{26}$$

The solution set which makes $I_{xy}^{(1)} = 0$ is a curve on the $x$-$y$ plane as shown by the dotted blue line in Fig. 3 for the chosen arbitrary array.

In order to choose a best point on this curve, the two important array design criteria are considered. The first criterion is the angular ambiguity where the steering vectors in (3) should be different for different DOA's. If they are similar for different DOA's, large ambiguity errors are likely to occur. So while searching the best solution for $I_{xy}^{(1)} = 0$, the azimuth angular ambiguity function in [23], which measures the similarity between steering vectors, should be minimized. The second criterion is the electromagnetic mutual coupling (MC) effect between the array elements. When the array elements are located close to each other, the MC distorts the array model

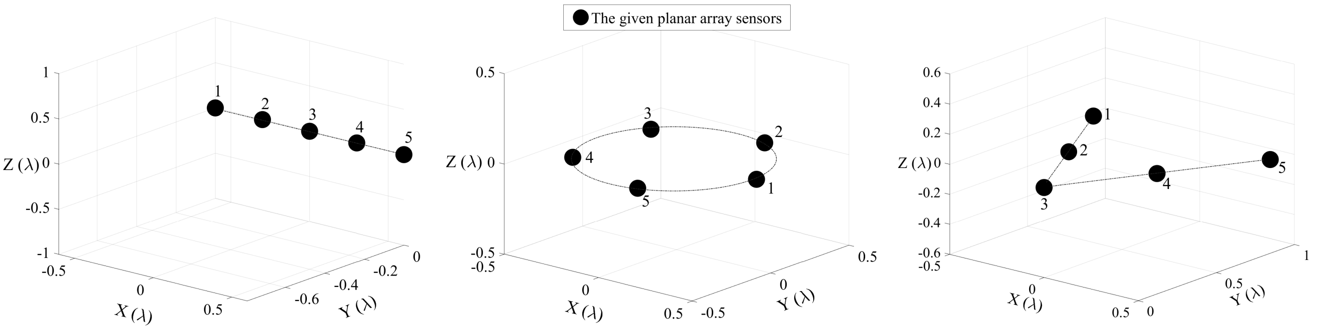


(a) (b) (c)

**FIGURE 2.** **The given arrays: (a) ULA, (b) UCA, and (c) V-shaped array.**

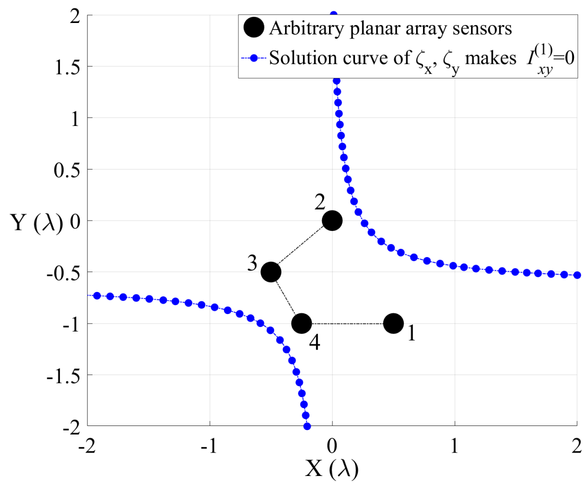


**FIGURE 3.** **The solution curve which makes $I_{xy}^{(1)} = 0$ in Step 1 for the given arbitrary array.**

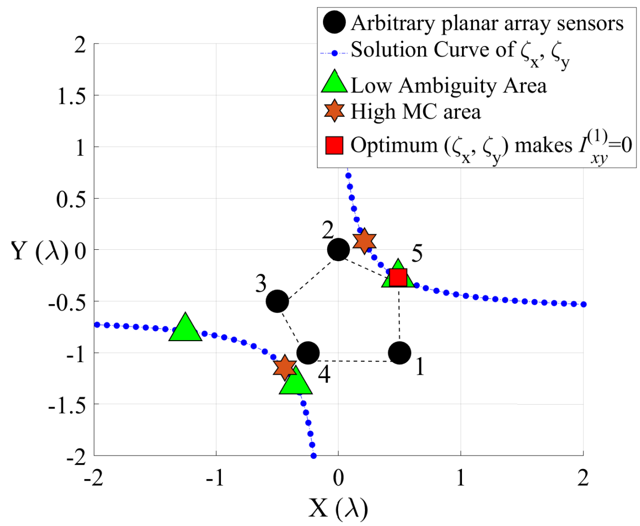


**FIGURE 4.** **Low ambiguity and high MC areas on the solution curve obtained by** (28) **in Step 1.**

in (1) [26]. We define the MC effect as a constraint in (28). The new sensor location problem is defined as the ambiguity and MC constrained minimization (optimization) problem which is presented in Section III-B.

### *B. AZIMUTH AMBIGUITY AND MC MINIMIZATION*

The normalized azimuth angle ambiguity function, defined in [23], is

$$\Lambda^{\theta}(\phi, \Delta\phi) = \frac{tr\left\{\mathbf{A}(\phi+\Delta\phi)^{H}\mathbf{A}(\phi)\right\}}{M^{(1)}L} \tag{27}$$

where $L$ is the number of the source signals.

This function measures the similarity between the steering vectors for different azimuth angles and gives values between 0 and 1 which means perfect orthogonal and collinear, respectively. We try to minimize this function while satisfying the zero cross moment-of-inertia constraint ($I_{xy}^{(1)} = 0$). Additionally, we define a new Mutual Coupling (MC) constraint for the new sensor to be added. The new sensor should not be located closer to any sensor in the array than $\lambda/4$. This distance restricts the MC effect at a reasonable level [22] and can be adjusted more precisely according to practical situations. Finally, we define the following constrained optimization cost function to get the optimum sensor location, $\left(\zeta_x, \zeta_y\right)$,

$$\begin{aligned} &\underset{\zeta_x,\zeta_y}{\text{minimize}} : \text{secondmax}\left\{\Lambda^{\theta}(\phi, \Delta\phi)\right\} \\ &\text{subject to} : \left\|\left(\zeta_x, \zeta_y\right) - (x_i, y_i)\right\| > \frac{\lambda}{4}, \quad i = 1, \ldots, M \\ &\qquad I_{xy}^{(1)} = 0; \end{aligned} \tag{28}$$

We have to minimize the side-lobe-levels (SLLs) (second max) for minimum ambiguity error with zero cross moment-of-inertia. For the given four-element arbitrary planar array in Fig. 4, the triangle markers show the minimum ambiguity locations which also make $I_{xy}^{(1)} = 0$. On the other hand, the hexagram markers, which are close to the array elements, show the high MC points. Hence the optimum location of the sensor to be added as a result of this optimization is marked with a square (■) marker for this example.

### C. STEP-2

In this step, we have to equalize the auto moment-of-inertia of coordinates ($I_{xx}$, $I_{yy}$, and $I_{zz}$) of a given array while keeping the $I_{xy}^{(1)} = 0$. We first find the largest auto moment-of-inertia and bring the rest to that value by adding new sensors.

$$\mathbb{I} = \max\left\{I_{xx}^{(1)},\ I_{yy}^{(1)},\ I_{zz}^{(1)}\right\} \tag{29}$$

where $\mathbb{I}$ is the maximum auto moment-of-inertia of $\mathbf{x}^{(1)}$, $\mathbf{y}^{(1)}$, and $\mathbf{z}^{(1)}$ coordinates given in (24).

Then, in order to equate $I_{xx}^{(1)}$, $I_{yy}^{(1)}$, $I_{zz}^{(1)}$ without changing the mean of $z$, we should add $N$ uniform sensors as follows,

$$\begin{aligned}
\mathbf{x}^{(2)} &= \left[\mathbf{x}^{(1)}\ d_x \mathbf{1}_N\right] \\
\mathbf{y}^{(2)} &= \left[\mathbf{y}^{(1)}\ d_y \mathbf{1}_N\right] \\
\mathbf{z}^{(2)} &= \left[\mathbf{z}^{(1)}\ d_z\left(\frac{(N+1)}{2} - i\right)\right]
\end{aligned} \tag{30}$$

where $i = 1, \ldots, N$, and $(\cdot)^{(2)}$ denotes the updated parameter at the second step. New auto moment-of-inertia of the updated $\mathbf{x}^{(2)}$, $\mathbf{y}^{(2)}$, and $\mathbf{z}^{(2)}$ coordinates where the derivation details are presented in Appendix VI-B, are obtained as,

$$I_{xx}^{(2)} = \frac{M^{(1)}N}{M^{(2)}} {d_x}^2 - \frac{{M^{(1)}}^2}{M^{(2)}} \mu_{\mathbf{x}^{(1)}}^2 - \frac{2M^{(1)}N}{M^{(2)}} \mu_{\mathbf{x}^{(1)}} d_x + \|\mathbf{x}^{(1)}\|^2 \tag{31}$$

$$I_{yy}^{(2)} = \frac{M^{(1)}N}{M^{(2)}} {d_y}^2 - \frac{{M^{(1)}}^2}{M^{(2)}} \mu_{\mathbf{y}^{(1)}}^2 - \frac{2M^{(1)}N}{M^{(2)}} \mu_{\mathbf{y}^{(1)}} d_y + \|\mathbf{y}^{(1)}\|^2 \tag{32}$$

$$I_{zz}^{(2)} = \frac{N\left(N^2-1\right)}{12} {d_z}^2 - \frac{{M^{(1)}}^2}{M^{(2)}} \mu_{\mathbf{z}^{(1)}}^2 + \|\mathbf{z}^{(1)}\|^2 \tag{33}$$

where $M^{(2)} = M^{(1)} + N$. $\mu_{\mathbf{x}^{(2)}}$, $\mu_{\mathbf{y}^{(2)}}$ and $\mu_{\mathbf{z}^{(2)}}$ are the updated mean of coordinates at the second step,

$$\begin{aligned}
\mu_{\mathbf{x}^{(2)}} &= \frac{M^{(1)}\mu_{\mathbf{x}^{(1)}} + Nd_x}{M^{(2)}}, \quad \mu_{\mathbf{y}^{(2)}} = \frac{M^{(1)}\mu_{\mathbf{y}^{(1)}} + Nd_y}{M^{(2)}} \\
\mu_{\mathbf{z}^{(2)}} &= \frac{M^{(1)}\mu_{\mathbf{z}^{(1)}}}{M^{(2)}}
\end{aligned} \tag{34}$$

The following three equations are solved for the unknowns $d_x$, $d_y$, and $d_z$,

$$I_{xx}^{(2)} - \mathbb{I} = 0, \quad I_{yy}^{(2)} - \mathbb{I} = 0, \quad I_{zz}^{(2)} - \mathbb{I} = 0 \tag{35}$$

Finally, the locations of the new additional $N$ sensors in (30) equalize the auto moment-of-inertia of coordinates. These sensors are marked with a diamond (♦) marker in Fig. 5 for ULA, UCA, V-shaped, and an arbitrary planar array for $N = 2$. We observed that adding new sensors to the $z$-axis affects the elevation angle ambiguity performance and the MC effect. Therefore, it is possible to examine the elevation angle ambiguity performance and the MC effect while selecting the optimum $N$ which is presented in Section III-D.

This procedure can be applied for all uniform/nonuniform linear and planar arrays. The proposed two-step algorithm is presented in Algorithm 1 for all the arrays located on the $x$-$y$ plane.

**Algorithm 1:** Pseudo-Code for the Proposed Algorithm

```
Step 1: Check cross moment-of-inertia between x and y coordinates
Input: x, y, z, M
Output: x^(1), y^(1), z^(1), M^(1)
if I_xy = 0 then
    x^(1) = x, y^(1) = y, z^(1) = z, M^(1) = M
    go to Step 2
else
    Find the optimum (ζ_x, ζ_y) using (28)
    Update sensor coordinates (24) and other
      parameters (25), (26)
Step 2: Equate auto moment-of-inertia of coordinates
Input: x^(1), y^(1), z^(1), M^(1), N
Output: x^(2), y^(2), z^(2), M^(2)
if I_xx^(1) ≠ I_yy^(1) ≠ I_zz^(1) then
    Find the largest auto moment-of-inertia via (29)
    Solve (35) to find d_x, d_y and d_z
    Update sensor coordinates (30) and other parameters
      (31)-(34)
```

### D. ELEVATION AMBIGUITY ANALYSIS

In order to extend arbitrary arrays by this approach, the number of array elements and added sensors should respectively satisfy $M \geq 2$ and $N \geq 2$ [24]. We can prefer a minimum number of additional sensors ($N = 2$) (to minimize array cost) while designing a volumetric array. On the other hand, although the number of sensors ($N$) added on the $z$-axis does not affect the azimuth ambiguity, these sensors will affect elevation ambiguity performance. The elevation angle ambiguity function can be written similarly to (27) with only $M^{(2)}$ instead of $M^{(1)}$. This function can be used as a performance criterion for choosing the appropriate number of added sensors in Step 2. If we choose $N$ too small, the elevation ambiguity performance may deteriorate as the distance between the sensors increases too much. But if we choose $N$ too large, the sensors on the $z$-axis become very close to each other. Thus, the MC effect arises. Consequently, there is a trade-off while choosing $N$. The graphical representation of the elevation angle ambiguity analysis for the arbitrary array given in Fig. 5(d) is shown in Fig. 6.

The figure shows that increasing the number of added sensors to the $z$-axis decreases the distance between the sensors ($d_z(\lambda)$) which increases the MC. However, the elevation angle ambiguity (side-lobe peak gain) decreases. It is possible to choose $N = 2$, but for the best results while taking into account the MC and ambiguity errors, choose $N$ between 3 and 6 (see Fig. 6) for the given array in Fig. 5(d).

## IV. SIMULATION RESULTS

In this part, we consider ULA, UCA, and V-shaped arrays and an arbitrary planar array in Fig. 2 and 3, respectively in order to show the performances of the extended volumetric arrays

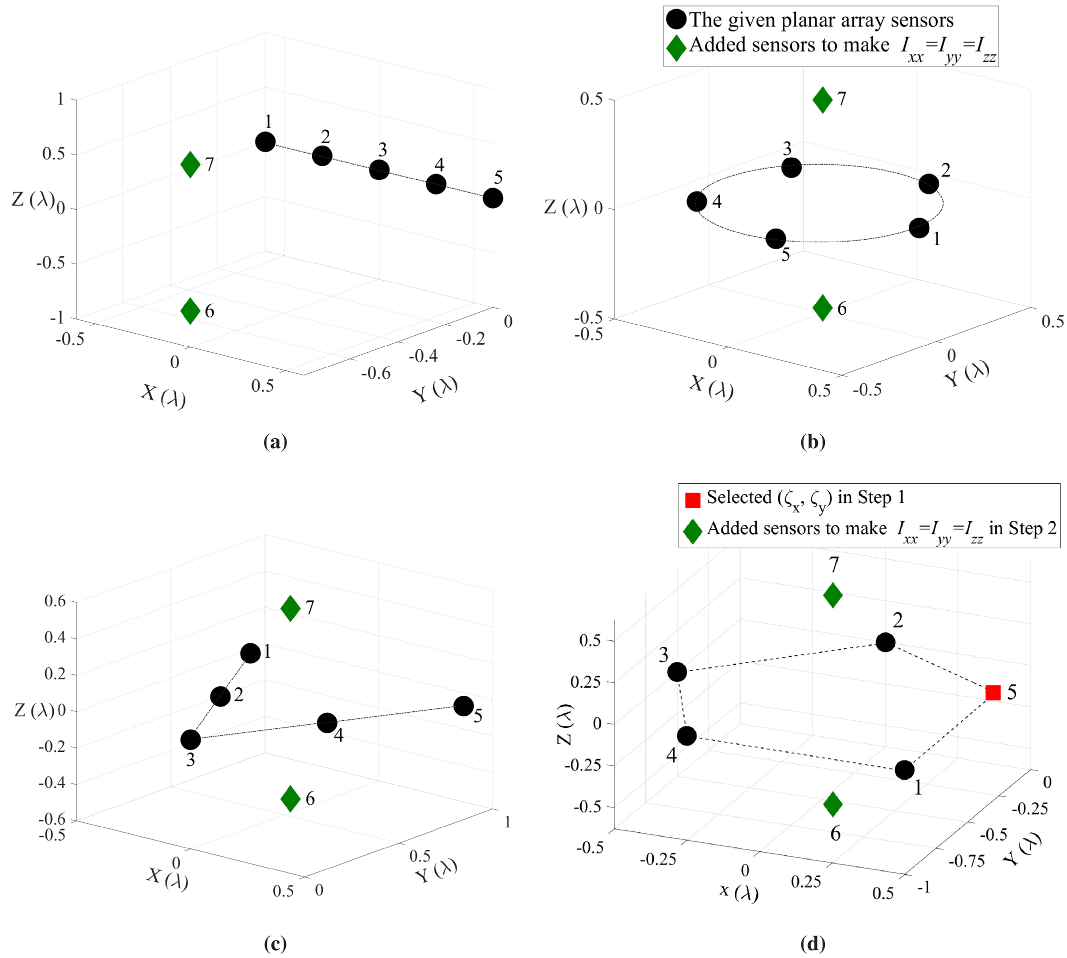


**FIGURE 5.** **The proposed 2-D isotropic volumetric arrays with inserted additional sensors (◆) on the $z$-axis of (a) ULA, (b) UCA, (c) V-shaped, and (d) Arbitrary arrays.**

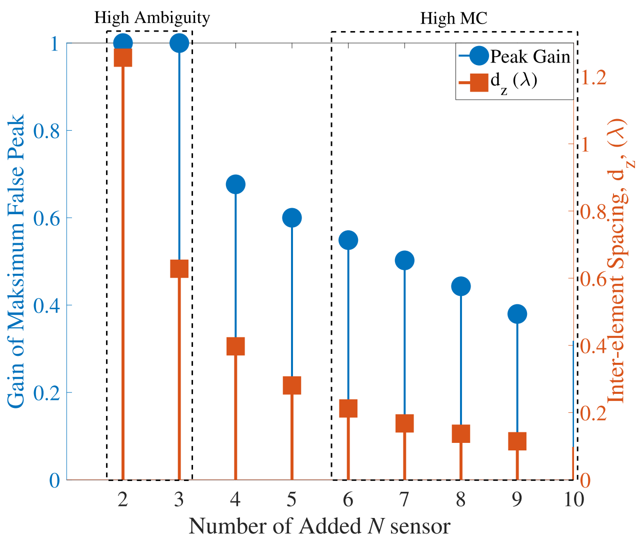


**FIGURE 6.** **The gain of the highest false peak and inter-element spacing, $d_z$, corresponding the number of added sensor on the $z$-axis in Step 2.**

for different cases. All the exact sensor locations are given in Table 1 in Appendix VI-C. The elements of the given planar array are denoted by circle markers (●) for $M = 5$ sensors. If a sensor is added in step 1, it is shown by a square (■) marker. Each sensor added in step 2 is shown by a diamond (◆) marker. Furthermore, for a fair comparison, the same total number of arrays elements are chosen.

In simulations, a single far-field source is assumed for DOA estimation. The source direction is represented as $(\phi_l, \theta_l)$, where $\phi \in [0, 180°]$ and $\theta \in [0, 90°]$ denote its azimuth and elevation angles in degrees, respectively as shown in Fig. 1. While azimuth performance of the array is tested, the elevation angle of the source is fixed at 85°, and while elevation performance of the array is tested, the azimuth angle of the source is fixed at 15°. CRLB values are obtained for the 256 snapshots (i.e. $T = 256$) and signal-to-noise ratio (SNR) of 20 dB. CRLB expressions given by (13) and (14) state the lowest achievable error variance of the unbiased azimuth and elevation estimators, respectively [1].

Fig. 7 shows the azimuth and elevation CRLB levels for given ULA, UCA, and V-shaped arrays and their volumetric versions obtained by the proposed algorithm. For the given planar arrays, the elevation errors go to infinity when the elevation angle approaches 90° as seen in Fig. 7(b). The proposed array design approach adds sensors to make both the azimuth and elevation CRLB levels equal over the

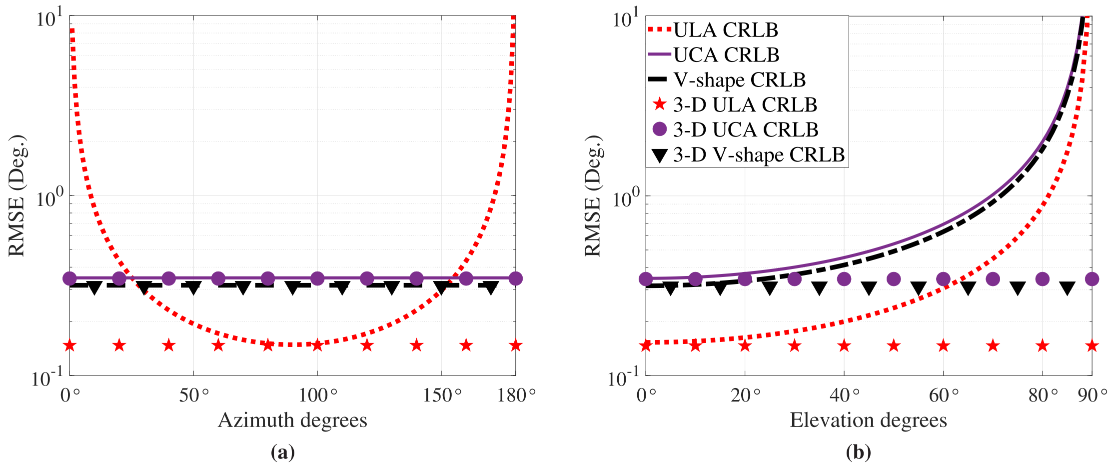


**FIGURE 7.** CRLB results: (a) Azimuth Performance ($\theta_{fixed} = 85°$) (b) Elevation performance ($\phi_{fixed} = 15°$).

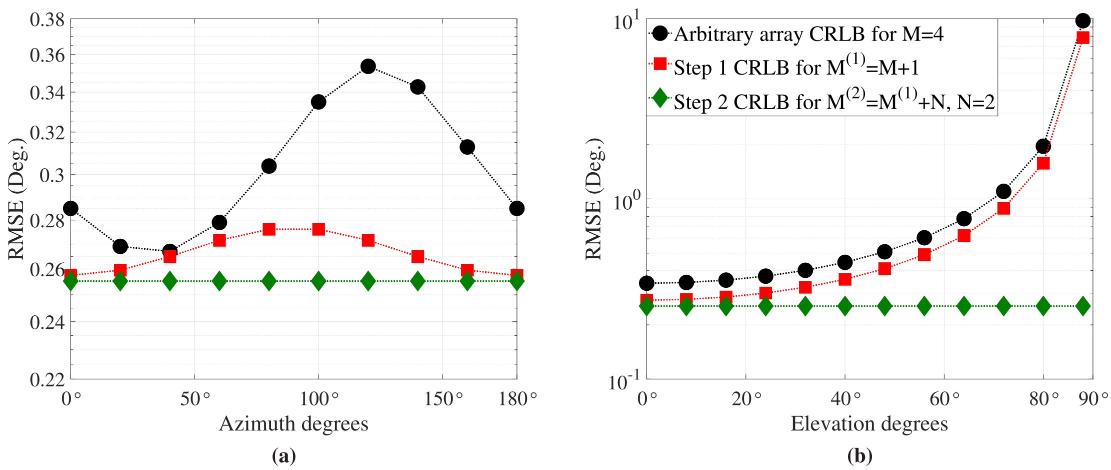


**FIGURE 8.** CRLB results of each step: (a) Azimuth performances ($\theta_{fixed} = 85°$) (b) Elevation performances ($\phi_{fixed} = 15°$).

entire azimuth/elevation angle range. Since these three arrays have zero cross-moments, (22) is satisfied and proceeded with the second step of Algorithm 1 (Step 2). In this step, the locations of $N$ new additional sensors, (30), are solved for the minimum possible number of sensors as $N = 2$. In Fig. 5(a), (b), and (c) newly added sensors are marked with the diamond marker (♦) to satisfy the (23) for ULA, UCA, and V-shaped arrays, respectively. The corresponding CRLB levels for these extended volumetric arrays are shown in Fig. 7(a) and (b) step by step. As it is shown, both the azimuth and elevation CRLB levels are equal for all the azimuth/elevation angles.

To verify that the proposed algorithm works for all linear and planar arrays, we arbitrarily choose four sensor locations on the planar array as shown in Fig. 3 with circle markers (●). This arbitrary array does not satisfy both the cross and auto moment-of-inertia conditions, (22) and (23), respectively. If we apply the algorithm, in the first step a solution curve on the $x$-$y$ plane which makes the cross moment-of-inertia to zero is created. The optimum sensor location $(\zeta_x, \zeta_y)$, which is marked by a square (■) on this curve, is the solution of the (28). This solution guarantees the mutual coupling and $I_{xy} = 0$ constraints while keeping the angular ambiguity minimum. In the second step of the algorithm two new sensors, which are marked as diamond (♦) as shown in Fig. 5(d), are added to equate the auto moment-of-inertia of coordinates. Fig. 8(a) and (b) show the azimuth and elevation CRLB levels of the arbitrary planar array before and after applying the array design approach for both azimuth and elevation isotropic performance. The effect of the progressively added sensors to CRLB levels in step one and two are also shown in 8(a) and (b), respectively.

The effect of the ambiguity errors is also investigated by using the two dimensional (2-D) Multiple Signal Classification (MUSIC) [25] algorithm. The MUSIC spectrum is calculated as,

$$\mathbf{P}_{MU}(\phi, \theta) = \frac{1}{\mathbf{a}^H(\phi_l, \theta_l)\,\mathbf{S}_\eta \mathbf{S}_\eta^H \mathbf{a}(\phi_l, \theta_l)} \tag{36}$$

where $\mathbf{S}_\eta$ corresponds to the noise subspace of the eigenvector matrix. $L$ highest peaks of $\mathbf{P}_{MU}(\phi, \theta)$ will be DOA angles of source signals.

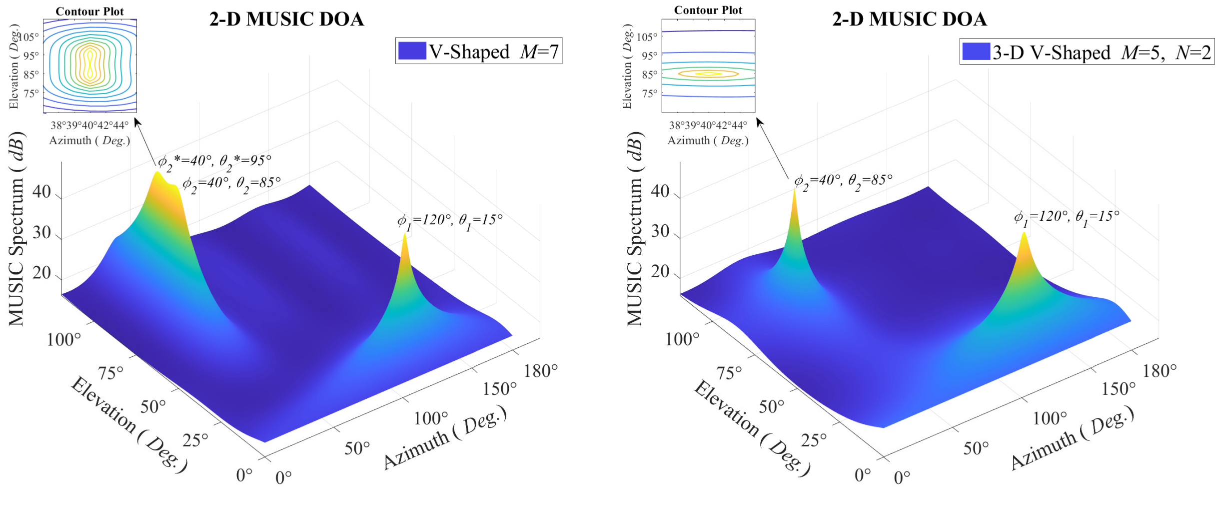


(a) (b)

**FIGURE 9.** 2-D MUSIC spectrum for (a) the planar V-Shaped and (b) proposed 3-D V-Shaped arrays.

In order to see 2-D DOA estimation performance of the designed array, an example of the 2-D MUSIC algorithm applied to the planar V-shaped [16] and proposed 3-D V-shaped arrays as shown in Fig. 9(a) and (b), respectively. In simulations, 100 Monte Carlo trials are performed to estimate $L = 2$ uncorrelated sources located at $(40°, 85°)$ and $(120°, 15°)$ for 5 dB SNR.

It can be seen that the planar V-shaped and proposed 3-D V-shaped arrays have almost the same performance for a low elevation angle with any azimuth angle. Nonetheless, the proposed volumetric array geometry overwhelmingly outperforms the planar V-shaped array after a certain elevation angle. Although the proposed 3-D V-shaped array estimates the second source $(40°, 85°)$ correctly without SLLs (see Fig. 9(b)), the given planar V-shaped array can not accurately estimate as well as creating high SLLs (see Fig. 9(a)).

## V. CONCLUSION

In this paper, an optimum and practical array extension algorithm is proposed for 2-D isotropic DOA estimation. The proposed approach can be applied to all arbitrary linear and planar arrays. In simulations, we applied the proposed design algorithm to well known ULA, UCA, V-shaped, and an arbitrary planar array. It is shown that for the selected arrays, the proposed volumetric array extension procedure improves the elevation estimation performances of these arrays (2-D isotropic) by considering both the angular ambiguity and mutual coupling effects with a minimum number of additional sensors. Thanks to its 2-D isotropic estimation performance, obtained arrays can be used as a benchmark array configuration for upcoming 2-D DOA estimation or beamforming algorithms. Besides, the proposed 2-D isotropic arrays can be considered for MIMO radar, acoustic, and smart antenna applications.

## VI. APPENDICES

### A. DERIVATION OF CROSS MOMENT-OF-INERTIA

Let's assume that we have given a planar array with coordinates as in (15). And then, assume that we add an additional sensor, then updated coordinates as in (24).

Mean of updated coordinates,

$$\mu_{\mathbf{x}^{(1)}} = \frac{\mathbf{x}^{(1)}\mathbf{1}_{M^{(1)}}^T}{M^{(1)}} = \frac{M\mu_{\mathbf{x}} + \zeta_x}{M^{(1)}} \tag{37}$$

$$\mu_{\mathbf{y}^{(1)}} = \frac{\mathbf{y}^{(1)}\mathbf{1}_{M^{(1)}}^T}{M^{(1)}} = \frac{M\mu_{\mathbf{y}} + \zeta_y}{M^{(1)}} \tag{38}$$

The cross moment-of-inertia between updated $\mathbf{x}^{(1)}$ and $\mathbf{y}^{(1)}$ coordinates is,

$$\begin{aligned}
I_{xy}^{(1)} &= \left(\mathbf{x}^{(1)} - \mu_{\mathbf{x}^{(1)}}\mathbf{1}_{M^{(1)}}\right)\left(\mathbf{y}^{(1)} - \mu_{\mathbf{y}^{(1)}}\mathbf{1}_{M^{(1)}}\right)^T \\
&= \left(x_1 - \mu_{\mathbf{x}^{(1)}}\right)\left(y_1 - \mu_{\mathbf{y}^{(1)}}\right) + \dots \\
&\quad + \left(x_M - \mu_{\mathbf{x}^{(1)}}\right)\left(y_M - \mu_{\mathbf{y}^{(1)}}\right) \\
&\quad + \left(\zeta_x - \mu_{\mathbf{x}^{(1)}}\right)\left(\zeta_y - \mu_{\mathbf{y}^{(1)}}\right) \\
&= x_1y_1 - x_1\mu_{\mathbf{y}^{(1)}} - y_1\mu_{\mathbf{x}^{(1)}} + \mu_{\mathbf{x}^{(1)}}\mu_{\mathbf{y}^{(1)}} + \dots + x_My_M \\
&\quad - x_M\mu_{\mathbf{y}^{(1)}} - y_M\mu_{\mathbf{x}^{(1)}} + \mu_{\mathbf{x}^{(1)}}\mu_{\mathbf{y}^{(1)}} + \zeta_x\zeta_y - \zeta_x\mu_{\mathbf{y}^{(1)}} \\
&\quad - \zeta_y\mu_{\mathbf{x}^{(1)}} + \mu_{\mathbf{x}^{(1)}}\mu_{\mathbf{y}^{(1)}} \\
&= \mathbf{x}\mathbf{y}^T - \mu_{\mathbf{y}^{(1)}}\mathbf{x}\mathbf{1}_M^T - \mu_{\mathbf{x}^{(1)}}\mathbf{y}\mathbf{1}_M^T + M^{(1)}\mu_{\mathbf{x}^{(1)}}\mu_{\mathbf{y}^{(1)}} \\
&\quad + \zeta_x\zeta_y - \zeta_x\mu_{\mathbf{y}^{(1)}} - \zeta_y\mu_{\mathbf{x}^{(1)}}
\end{aligned} \tag{39}$$

Substitute (37) and (38) into (39), and recall (21) as $\mathbf{x}\mathbf{1}_M^T = M\mu_{\mathbf{x}}$, thus,

$$\begin{aligned}
I_{xy}^{(1)} &= \mathbf{x}\mathbf{y}^T - \frac{M\mu_{\mathbf{y}} + \zeta_y}{M^{(1)}}M\mu_{\mathbf{x}} - \frac{M\mu_{\mathbf{x}} + \zeta_x}{M^{(1)}}M\mu_{\mathbf{y}} \\
&\quad + M^{(1)}\frac{M\mu_{\mathbf{x}} + \zeta_x}{M^{(1)}}\frac{M\mu_{\mathbf{y}} + \zeta_y}{M^{(1)}} \\
&\quad + \zeta_x\zeta_y - \zeta_x\frac{M\mu_{\mathbf{y}} + \zeta_y}{M^{(1)}} - \zeta_y\frac{M\mu_{\mathbf{x}} + \zeta_x}{M^{(1)}}
\end{aligned}$$

$$
\begin{aligned}
&= \mathbf{x}\mathbf{y}^T - \frac{M^2\mu_{\mathbf{x}}\mu_{\mathbf{y}}}{M^{(1)}} - \frac{M\mu_{\mathbf{x}}\zeta_y}{M^{(1)}} - \frac{M^2\mu_{\mathbf{x}}\mu_{\mathbf{y}}}{M^{(1)}} \\
&\quad - \frac{M\mu_{\mathbf{y}}\zeta_x}{M^{(1)}} + \frac{M^2\mu_{\mathbf{x}}\mu_{\mathbf{y}}}{M^{(1)}} + \frac{M\mu_{\mathbf{x}}\zeta_y}{M^{(1)}} + \frac{M\mu_{\mathbf{y}}\zeta_x}{M^{(1)}} \\
&\quad + \frac{\zeta_x\zeta_y}{M^{(1)}} + \zeta_x\zeta_y - \frac{M\mu_{\mathbf{y}}\zeta_x}{M^{(1)}} - \frac{\zeta_x\zeta_y}{M^{(1)}} - \frac{M\mu_{\mathbf{x}}\zeta_y}{M^{(1)}} - \frac{\zeta_x\zeta_y}{M^{(1)}} \\
&= \mathbf{x}\mathbf{y}^T + \frac{M}{M^{(1)}}\zeta_x\zeta_y - \frac{M^2}{M^{(1)}}\mu_{\mathbf{x}}\mu_{\mathbf{y}} - \frac{M}{M^{(1)}}\mu_{\mathbf{y}}\zeta_x \\
&\quad - \frac{M}{M^{(1)}}\mu_{\mathbf{x}}\zeta_y \qquad (40)
\end{aligned}
$$

This completes the proof.

### B. DERIVATION OF AUTO MOMENT-OF-INERTIA

The auto moment-of-inertia of $\mathbf{x}^{(2)}$, is,

$$
\begin{aligned}
I_{xx}^{(2)} &= \|\mathbf{x}^{(2)} - \mu_{\mathbf{x}^{(2)}}\mathbf{1}_{M^{(2)}}\|^2 \\
&= \left(x_1 - \mu_{\mathbf{x}^{(2)}}\right)^2 + \left(x_2 - \mu_{\mathbf{x}^{(2)}}\right)^2 + \cdots + \left(x_M - \mu_{\mathbf{x}^{(1)}}\right)^2 \\
&\quad + \left(\zeta_x - \mu_{\mathbf{x}^{(2)}}\right)^2 + N\left(d_x - \mu_{\mathbf{x}^{(2)}}\right)^2 \\
&= x_1^2 + x_2^2 + \cdots + x_M^2 + \zeta_x^2 + Nd_x^2 \\
&\quad - 2\mu_{\mathbf{x}^{(2)}}^2 \underbrace{\left(x_1 + x_2 \ldots x_M + \zeta_x + Nd_x\right)}_{M^{(2)}\mu_{\mathbf{x}^{(2)}}^2} + M^{(2)}\mu_{\mathbf{x}^{(2)}}^2 \\
&= \|\mathbf{x}^{(1)}\|^2 + Nd_x^2 - M^{(2)}\mu_{\mathbf{x}^{(2)}}^2 \qquad (41)
\end{aligned}
$$

Substituting (34) into (41) yields,

$$
I_{xx}^{(2)} = \frac{M^{(1)}N}{M^{(2)}}d_x{}^2 - \frac{M^{(1)2}}{M^{(2)}}\mu_{\mathbf{x}^{(1)}}^2 - \frac{2M^{(1)}N}{M^{(2)}}\mu_{\mathbf{x}^{(1)}}d_x + \|\mathbf{x}^{(1)}\|^2 \qquad (42)
$$

$I_{yy}^{(1)}$ and $I_{zz}^{(1)}$ can be obtained in the same way. This completes the proof.

### C. SENSOR ARRAY COORDINATES

**TABLE 1. The Coordinates of Sensors in Terms of the wavelength (λ).**

| Arrays | | Planar array sensors (●) 1st | 2nd | 3rd | 4th | 5th | Added sensor (♦) 6th | 7th |
|---|---|---|---|---|---|---|---|---|
| | x | -1.00 | -0.50 | 0.00 | 0.50 | 1.00 | 0.00 | 0.00 |
| 3-D | y | 0.00 | 0.00 | 0.00 | 0.00 | 0.00 | -1,32 | -1,32 |
| ULA | z | 0.00 | 0.00 | 0.00 | 0.00 | 0.00 | 1,11 | -1,11 |
| | x | 0.42 | 0.13 | -0.34 | -0.34 | 0.13 | 0.00 | 0.00 |
| 3-D | y | 0.00 | 0.40 | 0.25 | -0.25 | -0.40 | 0.00 | 0.00 |
| UCA | z | 0.00 | 0.00 | 0.00 | 0.00 | 0.00 | -0.47 | 0.47 |
| | x | -0.46 | -0.23 | 0.00 | 0.23 | 0.46 | 0.00 | 0.00 |
| 3-D | y | 0.88 | 0.44 | 0.00 | 0.44 | 0.88 | 0.53 | 0.53 |
| V | z | 0.00 | 0.00 | 0.00 | 0.00 | 0.00 | -0.52 | 0.52 |
| | | | | | | (■) | (♦) | (♦) |
| | x | 0.50 | 0.00 | -0.50 | -0.25 | 0.488 | 0.047 | 0.047 |
| 3-D | y | -1.00 | 0.00 | -0.50 | -1.00 | -0.27 | -0.526 | -0.526 |
| Arb. | z | 0.00 | 0.00 | 0.00 | 0.00 | 0.00 | -0.628 | 0.628 |

## REFERENCES


[1] A. J. Weiss and B. Friedlander, "On the Cramér–Rao bound for direction finding of correlated signals," *IEEE Trans. Signal Process.*, vol. 41, no. 1, pp. 495–499, Jan. 1993.

[2] H. Gazzah and S. Marcos, "Analysis and design of (non-)isotropic arrays for 3D direction finding," in *Proc. IEEE/SP 13th Workshop Stat. Signal Process.*, Novosibirsk, Russia, Jul. 2005, pp. 491–496.

[3] H. Gazzah and K. Abed-Meraim, "Optimum ambiguity-free directional and omnidirectional planar antenna arrays for DOA estimation," *IEEE Trans. Signal Process.*, vol. 57, no. 10, pp. 3942–3953, Oct. 2009.

[4] M. Gavish and A. J. Weiss, "Array geometry for ambiguity resolution in direction finding," *IEEE Trans. Antennas Propag.*, vol. 44, no. 6, pp. 889–895, Jun. 1996.

[5] U. Baysal and R. L. Moses, "Optimal array geometries for wideband DOA estimation," in *Proc. MSS Meeting Battlefield Acoustic Seismic Sensors*, Laurel, MD, USA, Oct. 2001, pp. 1–13.

[6] R. O. Nielsen, "Azimuth and elevation angle estimation with a three-dimensional array," *IEEE J. Ocean. Eng.*, vol. 19, no. 1, pp. 84–86, Jan. 1994.

[7] M. Hawkes and A. Nehorai, "Effects of sensor placement on acoustic vector-sensor array performance," *IEEE J. Ocean. Eng.*, vol. 24, no. 1, pp. 33–40, Jan. 1999.

[8] H. Chen, X. Li, and Z. Zhuang, "Antenna geometry conditions for MIMO radar with uncoupled direction estimation," *IEEE Trans. Antennas Propag.*, vol. 60, no. 7, pp. 3455–3465, Jul. 2012.

[9] X. Wang, E. Aboutanios, and M. G. Amin, "Adaptive array thinning for enhanced DOA estimation," *IEEE Signal Process. Lett.*, vol. 22, no. 7, pp. 799–803, Jul. 2015.

[10] Ü. Baysal and R. L. Moses, "On the geometry of isotropic arrays," *IEEE Trans. Signal Process.*, vol. 51, no. 6, pp. 1469–1478, Jun. 2003.

[11] A. Ghani, F. Keyvani, and S. H. Sedighy, "Antenna array placement on limited bound for isotropic and optimal direction-of-arrival estimation," *IET Signal Process.*, vol. 12, no. 3, pp. 277–283, May 2018.

[12] T. Filik and T. E. Tuncer, "Uniform and nonuniform V-shaped isotropic planar arrays," in *Proc. 5th IEEE Sensor Array Multichannel Signal Process. Workshop*, Darmstadt, Germany, Jul. 2008, pp. 1–5.

[13] M. Koivisto, A. Hakkarainen, M. Costa, P. Kela, K. Leppanen, and M. Valkama, "High-efficiency device positioning and location-aware communications in dense 5G networks," *IEEE Commun. Mag.*, vol. 55, no. 8, pp. 188–195, Aug. 2017.

[14] M. M. Azari, H. Sallouha, A. Chiumento, S. Rajendran, E. Vinogradov, and S. Pollin, "Key technologies and system trade-offs for detection and localization of amateur drones," *IEEE Commun. Mag.*, vol. 56, no. 1, pp. 51–57, Jan. 2018.

[15] İ. Güvenç, O. Ozdemir, Y. Yapici, H. Mehrpouyan, and D. Matolak, "Detection, localization, and tracking of unauthorized UAS and jammers," in *Proc. IEEE/AIAA 36th Digit. Avionics Syst. Conf. (DASC)*, St. Petersburg, FL, USA, Sep. 2017, pp. 1–10.

[16] T. Filik and T. E. Tuncer, "Uniform and nonuniform V-shaped planar arrays for 2-D direction-of-arrival estimation," *Radio Sci.*, vol. 44, no. 5, pp. 1–12, Oct. 2009.

[17] D. T. Vu, A. Renaux, R. Boyer, and S. Marcos, "A Cramér–Rao bounds based analysis of 3D antenna array geometries made from ULA branches," *Multidimensional Syst. Signal Process.*, vol. 24, no. 1, pp. 121–155, Mar. 2013.

[18] F. Harabi, A. Gharsallah, and S. Marcos, "Three-dimensional antennas array for the estimation of direction of arrival," *IET Microw., Antennas Propag.*, vol. 3, no. 5, pp. 843–849, Aug. 2009.

[19] A. Dogandzic and A. Nehorai, "Cramér–Rao bounds for estimating range, velocity, and direction with an active array," *IEEE Trans. Signal Process.*, vol. 49, no. 6, pp. 1122–1137, Jun. 2001.

[20] R. Fitzpatrick, "Rigid body rotation," in *Newtonian Dynamics*, 4th ed. Raleigh, NC, USA: Lulu Enterprises, 2011, pp. 106–107.

[21] H. Goldstein, C. P. Poole, and J. L. Safko, *Classical Mechanics*, 3rd ed. Reading, MA, USA: Addison-Wesley, 2001, pp. 187–194.

[22] B. Friedlander and A. J. Weiss, "Direction finding in the presence of mutual coupling," *IEEE Trans. Antennas Propag.*, vol. 39, no. 3, pp. 273–284, Mar. 1991.

[23] M. Eric, A. Zejak, and M. Obradovic, "Ambiguity characterization of arbitrary antenna array: Type I ambiguity," in *Proc. IEEE 5th Int. Symp. Spread Spectr. Tech. Appl.*, Sun City, South Africa, vol. 2, Sep. 1998, pp. 399–403.

[24] L. C. Godara and A. Cantoni, "Uniqueness and linear independence of steering vectors in array space," *J. Acoust. Soc. Amer.*, vol. 70, no. 2, pp. 467–475, Aug. 1981.

[25] R. Schmidt, "Multiple emitter location and signal parameter estimation," *IEEE Trans. Antennas Propag.*, vol. AP-34, no. 3, pp. 276–280, Mar. 1986.

[26] T. Filik and T. E. Tuncer, "2-D DOA estimation in case of unknown mutual coupling for multipath signals," *Multidimensional Syst. Signal Process.*, vol. 27, no. 1, pp. 69–86, Jan. 2016.

**FESIH KESKIN** received the B.S. degree in electrical and electronics engineering from Firat University, in 2009, and the M.S. degree in electrical and electronics engineering from Anadolu University, in 2014. He is currently pursuing the Ph.D. degree with the Department of Electrical and Electronics Engineering, Eskisehir Technical University. His research interests include statistical signal processing, sensor array geometry design, and sensor array signal processing.

**TANSU FILIK** received the B.S. degree in electrical engineering from Anadolu University, in 2002, and the integrated M.S. and Ph.D. degrees in electrical engineering from Middle East Technical University (METU), in 2010. From 2002 to 2010, he was with the Sensor Array and Multichannel Signal Processing (SAM) Group, METU. From 2010 to 2012, he was with the Radar, Electronic Warfare and Intelligence Systems Division, Aselsan Inc. He is currently with the Department of Electrical and Electronics Engineering, Eskisehir Technical University. He is the Founder of the Sensor Array Signal Processing Laboratory, Department of Electrical and Electronics Engineering, Eskisehir Technical University. His research interest includes statistical signal processing, array signal processing, signal processing for communications, and renewable energy.